

Water Resources Research

TECHNICAL REPORTS: METHODS

10.1029/2021WR030249

Key Points:

- Approaches for solving upscaled water resources problems using quantum-like tools are explored using solute transport as an example
- Advective-dispersive transport in porous media is represented using probability amplitude functions instead of probability distributions
- Functions with identical probability densities may have different amplitudes, which embed a sub-continuum heterogeneity into the problem

Correspondence to:

N. B. Engdahl,
nick.engdahl@wsu.edu

Citation:

Engdahl, N. B. (2021). Using complex probability amplitudes to simulate solute transport in composite porous media. *Water Resources Research*, 57, e2021WR030249. <https://doi.org/10.1029/2021WR030249>


Received 19 APR 2021

Accepted 11 AUG 2021

© 2021. The Authors.

This is an open access article under the terms of the [Creative Commons Attribution-NonCommercial-NoDerivs License](https://creativecommons.org/licenses/by-nc-nd/4.0/), which permits use and distribution in any medium, provided the original work is properly cited, the use is non-commercial and no modifications or adaptations are made.

Using Complex Probability Amplitudes to Simulate Solute Transport in Composite Porous Media

Nicholas B. Engdahl¹ 

¹Civil and Environmental Engineering, Washington State University, Pullman, WA, USA

Abstract Probability amplitudes are fundamental to quantum mechanics and offer robust descriptions of complicated systems, which have allowed physicists to explain behaviors inaccessible to classical physics. This article ponders how some of the same conceptual underpinnings of the mathematics used for modeling quantum systems might be applied to subsurface water resources problems and speculates how these tools could facilitate applications on quantum computers. A probability amplitude-based model for describing advective-dispersive transport in porous media using linear operators is investigated. The proposed complex valued model decomposes spreading into two “sub-continuum partial dispersion” coefficients, and this recovers classical spreading when the sum of these coefficients is the Fickian dispersion coefficient. However, the probability amplitudes have a many-to-one relationship to a probability distribution, so it embeds a level of heterogeneity into seemingly equivalent functions. Two propagators with different sub-continuum coefficients may have the same macroscopic behavior when either is considered in isolation, but when they act on the other the system’s behavior changes. Differences in the amplitudes cause a reduction in spreading as velocity correlations are disrupted, despite both propagators having identical dispersion coefficients, and this cannot be achieved using classical methods without changing the dispersion coefficient. The main point is that these amplitude-based models offer a way to embed information about the system into the propagators, instead of just “averaging it out” when making an upscaled model.

1. Introduction

Accurately modeling transport processes in heterogeneous porous media has been one of the longstanding challenges in water resources. The advection-dispersion equation (ADE) works well when the physical structure and heterogeneity of an aquifer are accurately resolved at scales commensurate with proper “representative elementary volumes” and these kinds of simulations can create highly complex transport behaviors (e.g., Engdahl & Weissmann, 2010; Green et al., 2010; Maxwell et al., 2009; Weissmann et al., 2002), but massive deviations from reality occur when the ADE is not applied properly. This has led to a wide range of “non-Fickian” behaviors that have been cataloged from simulations and experiments, and are often described using a variety of reduced dimensional, upscaled models. Examples of these include stochastic methods (Dagan, 1990; Gelhar & Axness, 1983; Neuman et al., 1987; Riva & Guadagnini, 2009; Simmons, 1982), immobile mass-transfer and integro-differential equations (memory functions) (Ginn et al., 2017; Haggerty & Gorelick, 1995; Silva et al., 2009), fractional derivatives (Zhang et al., 2007), and time domain random walks (Dentz et al., 2016; Massoudieh & Dentz, 2020; Sherman et al., 2020), to name but a few among a vast body of literature. In short, these models are necessary because information is lost when moving to larger scales and each type of non-Fickian model “puts back” some of this information with unique closures (for a comparison see Neuman & Tartakovsky, 2009). The current suite of non-Fickian techniques spans a dizzying range of methods and underlying theories, but absent from that list is the framework that has enabled some of the most profound scientific advances of the last century: quantum mechanics.

The general omission of quantum techniques from flow and transport modeling makes sense when taken at face value because the typical scales for quantum mechanical applications are orders of magnitude below that of continuum fluid mechanics. However, subsurface flow systems have some interesting similarities to quantum mechanical problems including minimum allowable scales (i.e., fluid continuum or Darcy continuum), being characterized in terms of their total energy, and high degrees of uncertainty; the reasons for this uncertainty are different in each field, but both are highly uncertain. The core of quantum mechanics is actually a tool set for describing observed phenomena that were outside the realm of what could be

described by classical physics (Bohm, 1951; McQuarrie & Simon, 1997). These tools happen to have been applied at molecular scales most of the time, but the mathematical tools themselves are not necessarily restricted to certain scales, rather to those problems with certain characteristics. Given such similarities, it seems reasonable to ask if something could be gained by adopting a “quantum-like” upscaled conceptual model for flow and transport, in addition to the basic question of feasibility. In a broader sense, this approach would not be describing sub-atomic or molecular scale processes in aquifers (doing so would be audaciously impractical), but rather could treat aquifers as inherently uncertain systems due to our lack of knowledge and describe their dynamics with mathematical tools similar to those used for quantum systems.

There is a second reason to consider quantum methods for water resources problems: the limitations of classical computers. Nonlinear solvers for complex water resource simulations have continued to advance by parallelizing the models, but these massive simulations (e.g., Hammond & Lichtner, 2010; Kollet et al., 2010; Maxwell et al., 2015) are usually so computationally intense that even sensitivity analysis becomes all but impossible. The next generation of high-performance simulations is likely to leverage quantum computers, but translating our models into these systems is not trivial due to their fundamentally different architectures (Johnston et al., 2019). Instead of trying to translate existing solvers into quantum algorithms, that might not even be efficient enough to merit translation, we could instead translate the mathematics of water resources problems into a quantum framework. The problems would then be posed in the natural language of quantum computers, facilitating rapid deployment as soon as fault-tolerant quantum computers are available. Such “quantum upscaled” groundwater flow or transport models are enticing because they could be incredibly fast, and also inescapably embed uncertainty in the simulations, but we must first ask if water resources problems can even be posed in quantum-like ways.

The purpose of this article is to explore how some of the mathematical tools used for quantum systems might be used in water resources using solute transport as a familiar and accessible entry point. The heart of any quantum system is a probability-amplitude known as the wave function (Bohm, 1951; Devanatham, 2011), and the primary objective herein is to demonstrate that a complex valued probability-amplitude function (PAF), or state function, can be defined to describe transport in the same manner as the ADE. It is shown that this state function recovers the Fickian model when certain conditions are satisfied, and also how the PAF can be evolved with linear operators in Section 3. The model has a many-to-one mapping of the PAFs onto the probability density function (PDF) solutions of the 1d ADE. This means that many different “sub-continuum” conditions can give rise to the same “macroscopic” behaviors because the PAFs retain different sub-continuum states instead of averaging them out. The most interesting feature of the amplitude-based model is that it can exhibit destructive interference that causes reduced spreading relative to the classical model. This implies that two kinds of porous media that are seemingly identical, based on a laboratory column test for example, can still be considered as distinct, but also that their interactions can impact results. Examples of these behaviors are presented as breakthrough curves and this constitutes (a) the first application of PAFs to ADE-type solute transport problems in porous media and (b) the first example of this kind of a complex, interaction-based mechanism for creating deviations from Fickian transport. This topic is theoretical, but the notion that additional information can be encoded in PAFs for flow and transport is potentially powerful. Similar methods could expand the possibilities for how subsurface flow and transport systems are represented mathematically, and this could help make progress toward quantum computer-based simulations for water resource problems.

2. Linear Operators for Solute Transport

Linear transfer functions (or more generally Green’s functions) in hydrology are common, particularly so in the case of environmental tracers as in the 1d equation

$$C(x,t) = \int_0^\infty \exp(-\lambda \tau) g(x,\tau) f(x,t - \tau) d\tau \quad (1)$$

where λ is a decay rate, g is the convolution kernel (often the residence time distribution), and f is some initial concentration distribution; here, we require that both g and f are PDFs. The same model is also the foundation of stochastic-convective transport (Ginn, 2001; Simmons, 1982; Simmons et al., 1995) and streamtube-based modeling of transport (Atchley et al., 2013; Cvetkovic et al., 2012; Loschko et al., 2016; Maxwell et al., 2003). The model embeds all transport into a single operator, g , which describes all changes

to f . Assuming $\lambda = 0$ for simplicity, the “linear” property becomes clear when Equation 1 is Laplace transformed in time

$$\tilde{C}(x,s) = \tilde{g}(x,s)\tilde{f}(x,s) \quad (2)$$

where \sim denotes a Laplace transformed (LT) function, s is the Laplace dual to time, and s is a complex variable ($s \in \mathbb{C}^1$). The kernel \tilde{g} is now written as a linear operator, or propagator, that acts on \tilde{f} , thus \tilde{g} changes the state of \tilde{f} to the state represented by \tilde{C} . The linear operator could also be defined in terms of its Fourier transform (see Appendix A), but the focus herein is primarily on the time domain since it generates breakthrough curves and this is suited to the one-sided LT.

2.1. Gaussian Model

The reference model for comparison will be a linear transfer function that represents advection and dispersion in a uniform porous medium according to a Gaussian Green’s function

$$g(t|x) = \frac{v}{\sqrt{4\pi Dt}} \exp\left[-\frac{(x-vt)^2}{4Dt}\right] \quad (3)$$

where D [L²/T] is the dispersion coefficient, and v [L/T] is the effective velocity, t [T] is time, all conditional to transport over the spatial scale x [L]; integrating Equation 3 over time shows it to be a PDF. Note that this is a slight departure from the common “simple solution” for diffusion with drift (e.g., Charbeneau, 2006) because of the presence of v in the numerator of the leading factor; this change is required to properly normalize under time integration but does not change the overall behavior. Adopting the breakthrough curve interpretation (a distribution over time at a fixed location), applying this propagator in sequential spatial steps of size $x \rightarrow \Delta x$ shows that the result of two steps of Δx in sequence is equivalent to a single step of size $2\Delta x$. Thus, $\tilde{C}(s|2\Delta x) = \tilde{g}(s|\Delta x)^2$, and application of the forward and inverse LT to Equation 3 proves it may also be generated from one application of $g(t|2\Delta x)$. If D or v , need to vary spatially, the model can be broken up into discrete steps where the parameters are constant since Equation 2 can be applied sequentially in a composite domain.

3. Probability Amplitudes for Advection-Dispersion

The concept of a probability amplitude comes from quantum theory where the wave function, $\psi(x,t)$, can provide a complete description of a quantum mechanical system (Bohm, 1951; McQuarrie & Simon, 1997). However, unlike $g(x,t)$, $\psi(x,t)$ is already a complex function (\mathbb{C}^d) so it may contain more information than $g(x,t)$. Conceptually, this is like distributing the probability density over another dimension, but this dimension is not directly observable. Specific functional forms of ψ describe specific systems, and the corresponding PDF, ρ , is found from

$$\rho'(x,t) = \psi^*(x,t)\psi(x,t) \quad (4a)$$

$$\rho(x,t) = \frac{\rho'(x,t)}{\int \rho'(x,t)dt} \quad (4b)$$

where $*$ denotes the complex conjugate. The ρ' notation is used to emphasize that the amplitude might not integrate to unity, but as long as the integral is finite it may be normalized with Equation 4b to generate a PDF (Devanatham, 2011); for compactness only ρ is used hereafter, which implies ρ' has already been normalized if necessary. The inclusion of a non-physical dimension (the complex parts of \mathbb{C}) provides the ability to describe, or perform, actions we otherwise cannot. These actions have physical consequences that can be observed, even if the underlying probability amplitude that causes them cannot be directly measured. Wave functions in quantum mechanics are usually applied to describe microscopic or smaller (molecular) phenomena like particle interactions in atoms, but here we ask if similar mathematical tools can be used for describing macroscopic flow and transport in porous media.

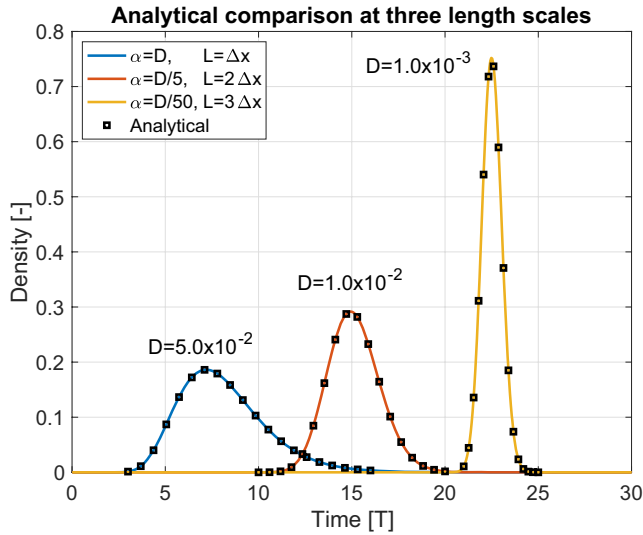


Figure 1. Comparison of the analytical solutions from Equation 3 (black squares) and Equation 4 through propagation with Equation 5 (lines) for three different length scales (L) and three different D coefficients. This shows that self-propagation of the probability-amplitude function model recovers the Fickian model.

The goal is to apply amplitude-based models for advection-dispersion processes but also to ask if a PAF approach might offer anything novel. First, a wave function must be defined, but hereafter “wave function” is replaced with “state function” to avoid any confusion with applied quantum mechanics; only the mathematics are being borrowed, not the physical interpretations. The state function will be required to be a complex valued amplitude that recovers Equation 3 when Equation 4 is applied. Many acceptable candidates likely exist, but just one acceptable PAF is needed to test the core concept. The following PAF is proposed as an *ad hoc* model for the state function

$$\psi(x,t) = \frac{\sqrt{v}}{[4\pi t(\alpha + \beta)]^{1/4}} \exp\left[\frac{-(x - vt)^2}{8t(\alpha + i\sqrt{\alpha\beta})}\right] \quad (5)$$

where $i = \sqrt{-1}$ and α and β are constant coefficients $\alpha, \beta \in \mathbb{R}$. Applying Equation 4, the resulting PDF of this state function is

$$\rho(x,t) = \psi^* \psi = \frac{v}{\sqrt{4\pi t(\alpha + \beta)}} \exp\left[\frac{-(x - vt)^2}{4t(\alpha + \beta)}\right] \quad (6)$$

and from this the equivalence to the advection-dispersion model (Equation 3) can be seen through $\alpha + \beta = D$, requiring $\alpha > 0$. Integration over time shows that Equation 6 is a PDF, so Equation 5 satisfies the fundamental requirement of a PAF, and it could also be interpreted as a wave packet (Bohm, 1951; Devanatham, 2011; Riazuddin, 2013). It should be noted that Equation 6 remains a Gaussian and all classical results and

analytical test cases (e.g., Carslaw & Jaeger, 1959; Ogata & Banks, 1961) will be recovered; as such, they are omitted here for brevity. A 1d model is adopted here for simplicity but extensions to 2- and 3d are presented in Appendix B.

The difference between this conceptual model and familiar Equation 3 is that macroscopic dispersion is formed as a combination of two “partial dispersion” factors, or “sub-continuum” coefficients, α and β . This is somewhat similar to a hydrodynamic interpretation of D where it is made up of an effective molecular diffusion coefficient and a dispersivity term; however, unlike Equation 3, Equation 5 keeps each term distinct.

Equation 5 is a Green’s function in terms of probability amplitudes and the state will be evolved over time where the propagator is applied at fixed spatial increments; this is called a “spatial propagator” since a continuous distribution over time is evolved over increments of 1d space (a “temporal” operator is presented in Appendix A). The result of these operations will be breakthrough curves at sequentially farther “downstream” locations. Lastly, since Equation 5 is not a unitary operator, the output of the linear operator(s) will need to be renormalized (i.e., Equation 4b to convert it to a PDF). The reason for this is that the leading factor (Equation 5) is not precisely the integral of the exponential term, so its probability mass is not unity. This was done so that Equation 3 (through Equation 6) is recovered in its normalized form because both Equations 5 and 6 cannot always be simultaneously normalized.

3.1. Recovery of the ADE

Next, consider how a system described with Equation 5 as the PAF can be evolved with linear operators analogously to the ADE (Equation 3) through Equation 2. Doing so will evolve a probability amplitude, $\psi(x,t) \in \mathbb{C}^1$, instead of a probability density, $g(x,t) \in \mathbb{R}^1$, though both operations are applied in the frequency domain. A single ψ propagating over a fixed length scale, Δx is given by

$$\tilde{\psi}(s|2\Delta x) = \tilde{\psi}(s|\Delta x)\tilde{\psi}(s|\Delta x) \quad (7)$$

and the PDF is recovered by normalizing the result of Equation 4.

The example problem showing these behaviors in Figure 1 uses $v = 0.4$, three different D values, and $\Delta x = 3$, applied over length scales $L = N\Delta x$ for $N = 1,2,3$; the initial condition, $N = 0$, is a Dirac-delta, $\delta(x, t = 0)$.

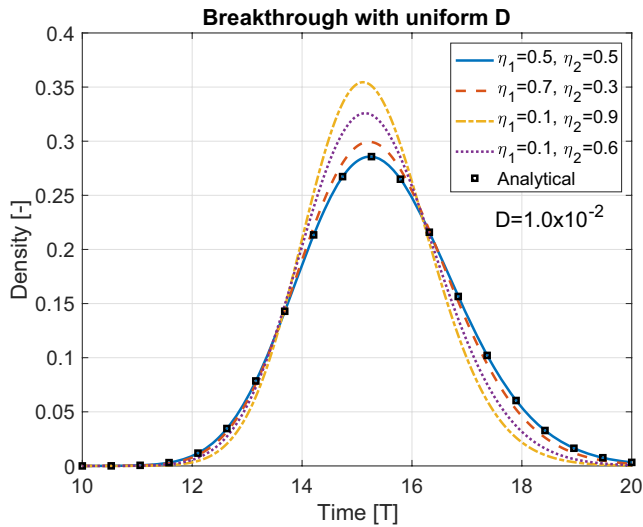


Figure 2. Example of uniform D propagators using different mixtures of α and β as reflected by η_j , requiring $\alpha_j + \beta_j = D$. Despite the fact that every propagator used in this example has an identical probability density function, the differences in the underlying amplitudes cause interference that decreases the spreading relative to the classical advection-dispersion equation model.

These three distances and Equation 3 comprise the reference solutions and values at selected times are shown as the black squares in Figure 1. The solutions for Equation 5, through Equation 6, are the solid lines, and are given for three values of the partial dispersion coefficients: $\alpha_1 = D$, $\alpha_2 = D/5$, and $\alpha_3 = D/50$, with the values of β defined from $\beta_j = D_j - \alpha_j$; the specific D values are different for each case and are listed in Figure 1. It should be clear that any α_j subject to $\alpha_j + \beta_j = D_j$ reproduces the classical model when the propagator acts on itself N times.

4. Interactions and Interference Across Interfaces

So far, a model has been proposed that has marginally greater complexity than classical analytical ADE models, and it has been shown that both the new and old models effectively do the same thing when a “Fickian equivalency condition” is satisfied, which is $\alpha + \beta = D$ ($\alpha > 0$). However, this curious PAF model makes some new behaviors possible. Recall that *any choice* of α and β that satisfy the Fickian equivalency condition give the same results, which is an expression of the many-to-one mapping of Equations 5–3, but what if two unique sets of α and β act on each other?

4.1. Uniform D

Define two spatial propagators, ψ_1 and ψ_2 , that have unique coefficient values that independently satisfy $\alpha_j + \beta_j = D$ for $j = 1, 2$. Conceptually, think of this as if transport were occurring in a column experiment where

the first half is full of material having ψ_1 and the other half is full of material having ψ_2 . The sequential operators are applied as before

$$\psi_{1 \rightarrow 2}(t|2\Delta x) = \mathcal{L}^{-1} \left[\tilde{\psi}_1(s|\Delta x) \tilde{\psi}_2(s|\Delta x) \right] \quad (8)$$

where \mathcal{L}^{-1} is the inverse LT operator, and the $1 \rightarrow 2$ subscript denotes the order of propagation. The resulting $\rho_{1 \rightarrow 2}$ no longer matches $C(t|2\Delta x)$, as shown in Figure 2. For simplicity, define $\alpha_j = \eta_j D$, so that $\beta_j = (1 - \eta_j)D$. Results for four sets of η_j are given in Figure 2 for $j = 1, 2$ where $j = 1$ is the first propagator in the sequence and $j = 2$ is the second. In every case where $\eta_1 \neq \eta_2$, the interaction of the different propagators reduces the amount of spreading relative to the Fickian model. Note that only one case of $\eta_1 = \eta_2$ is shown ($\eta = 0.5$) but any $\eta > 0$ value could have been used and would produce an identical result. An analytical example of this interference for a temporal propagator is provided in Appendix A.

Conceptually this example might represent a tracer moving through two different kinds of porous media that each have *identical macroscopic behavior*, but that have sub-continuum differences, which are encoded in their unique probability amplitude functions. This situation has clear physical connections in hydrogeology because sharp juxtapositions of similar material occur in abundance in fluvial and alluvial deposits, along cross-beds or anytime scour or erosional surfaces are filled back in. The key point is that *interactions* across interfaces change the overall behavior in this model despite the fact that both transfer functions have *identical* PDFs. Furthermore, this interaction will cause reduced spreading relative to D (see Appendix A) because the combined spreading rate cannot exceed that of the parts, mathematically or physically.

4.2. Variable D

Naturally, a follow-up question to the previous example is what happens when D also varies spatially along the sequence of propagation? The requirement of a single D is now relaxed and the approach generalized so that each propagator has its own unique value, D_j still subject to $D_j = \alpha_j + \beta_j$ for $j = 1, 2$, but also requiring $D_1 \neq D_2$. Conceptually, the laboratory column from before is now filled with two different kinds of porous

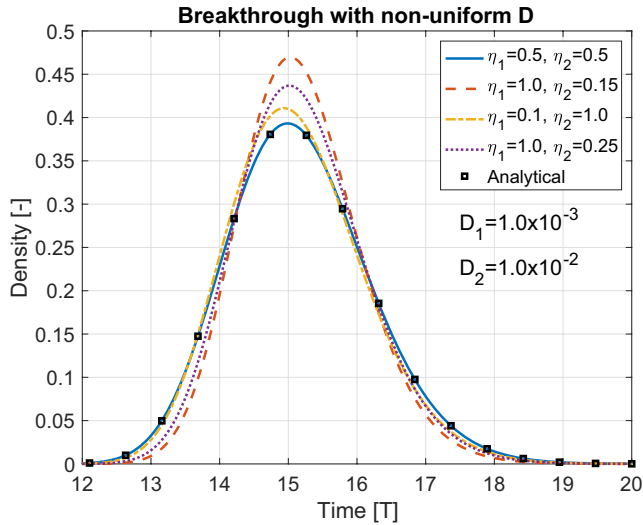


Figure 3. Example of nonuniform D propagators using different mixtures of α and β as reflected by η_j . The macroscopic behavior matches the real-space analytical solution (e.g., Equations 1 and 3) anytime $\eta_1 = \eta_2$, but if $\eta_1 \neq \eta_2$ interference causes the results to generate less spreading than the classical analytical solution.

media, arranged in series, and the solute moves out of ψ_1 , into ψ_2 , then out of the column.

The form of the propagator is still Equation 8, where $D_j \neq D_k$, and the corresponding breakthrough curves are shown in Figure 3 for different combinations of η . The key result is that, regardless of the specific values of D , anytime that $\eta_1 = \eta_2$, dispersion will proceed in the same manner predicted by the ADE without destructive interference. When $\eta_1 \neq \eta_2$, the upscaled, effective dispersion will not match that of either propagator will instead become a combination of their contributions that exhibits reduced spreading (Appendix A).

The relationship between the effective diffusion coefficient and the two sets of parameters can be determined analytically from Equation 5, which also follows from Appendix A. For simplicity, define $\zeta_j = \alpha_j + i\sqrt{\alpha_j\beta_j}$. After some algebra and complex conjugation, one finds

$$D' = \frac{\gamma\gamma^*}{\gamma + \gamma^*} \quad (9)$$

where $\gamma = \zeta_1 + \zeta_2$. The *relative* amount of dispersion caused by each amplitude component, η and $(1 - \eta)$ for α and β , respectively, dictates whether or not interference will occur, which is a fascinating property. However, this also suggests a way that these parameters might be defined experimentally when considering that $D_j = \alpha_j + \beta_j$. If $D_1 = D_2 \neq D'$, and all three values are measured, then the system of equations makes it

possible to express D' as a function of either the unknown α or β values, eliminating an unknown. Combining different materials in series and measuring their individual and “composite” D' values could be a practical way of estimating these coefficients. However, the main point is that the previously shown interference effects can be accurately predicted.

5. Numerical Example

The PAF-based model has been shown to work analytically and some possible mechanisms for its behavior in composite domains have been suggested, but what remains to be seen is whether or not the behavior suggested in Section 4.2 actually occurs. A numerical experiment was constructed based on two statistically identical domains that have different velocity fields. The hydraulic conductivity distributions were generated as log-normal random fields with correlation lengths of $\lambda_L = 1.0[L]$ and $\lambda_T = 0.15[L]$ in the longitudinal and transverse directions, respectively, with a geometric mean value of $\bar{k} = 1.0[L/T]$ and uniform porosity of 0.3. The 2d numerical flow cell was five dimensionless units long by two units wide using a uniform cell size of $\Delta x = \Delta y = 0.05[L]$ and was subjected to a hydraulic gradient of 5% parallel to the long axis with zero flux boundaries on the transverse edges. The velocity magnitude and potential contours of the flow fields for the two domains, Ω_1 and Ω_2 , respectively, are shown in Figure 4. Transport was simulated using random walk particle tracking with a uniform diffusion coefficient of $5.0 \times 10^{-3}[L^2/T]$ and an ensemble of 25k particles per domain placed at the inlet using a flux weighted distribution to represent the Green’s function response; higher numbers of particles did not change the results. The outflow boundary for the particles was an outward flux that allowed particles to exit the domain when they reached the end of the column. The effective velocity for the domains was $2.98[L/T]$ and this varied by less than 1% across the three numerical models. All times were normalized by the mean breakthrough to express them as nondimensional quantities (i.e., pore volumes) and lengths were normalized by the domain length.

Three numerical experiments were conducted: transport in each domain was simulated independently (simulations 1 and 2), then the two were lined up end-to-end in a double length experiment where Domain 1 flowed into Domain 2, precisely the same as the composite example in Section 4.2. Effective hydrodynamic dispersion coefficients were fit to each simulation for comparison (Figure 5): Domain 1 had $D_1 = 5.88 \times 10^{-2}$, Domain 2 had $D_2 = 5.68 \times 10^{-2}$, and Domain 1 flowing into Domain 2 had

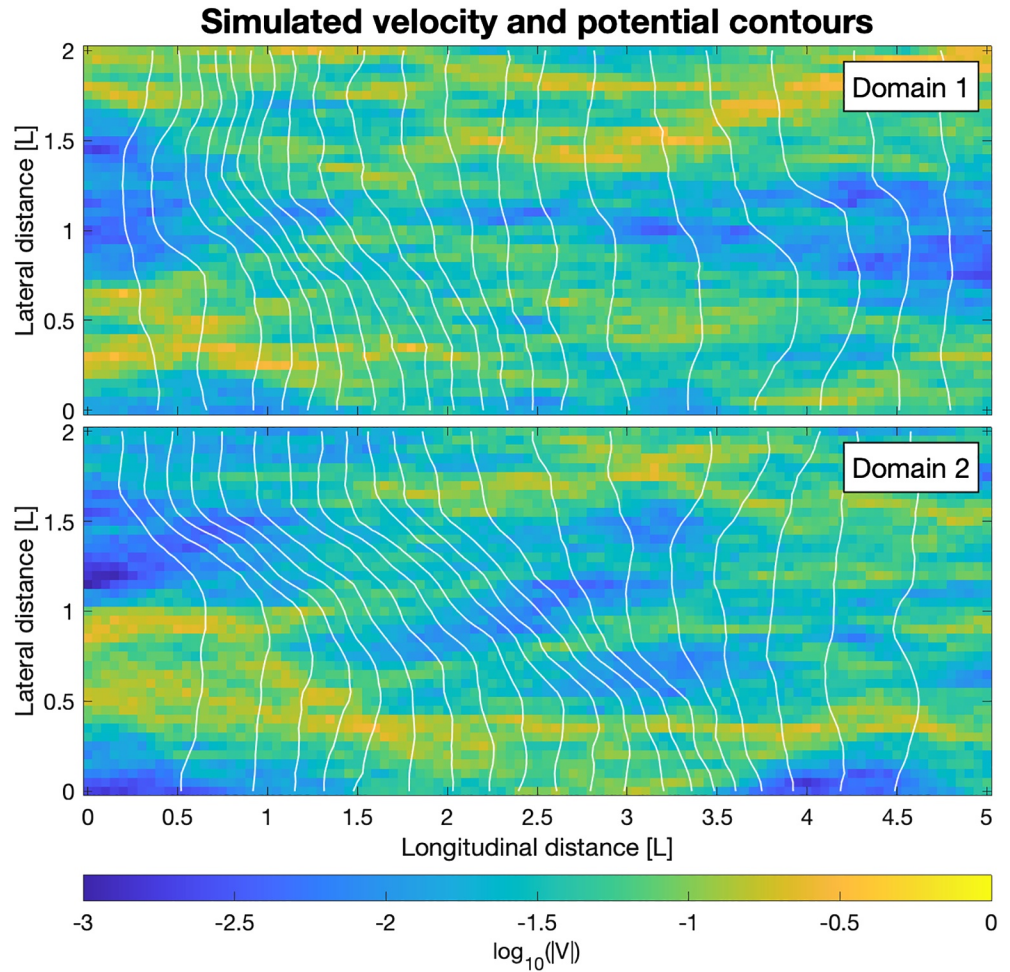


Figure 4. Velocity magnitude and potential contours for the two example domains used in the numerical validation exercise. Units are dimensionless. The composite simulation puts these domains end-to-end in an extended column experiment where Domain 1 flows into Domain 2.

$D_{1 \rightarrow 2} = 4.72 \times 10^{-2}$; recall that the BTCs were nondimensionalized so unit length and velocities were used in the fitting. Direct convolution of the breakthrough curves (BTCs) gave a curve with $D_{1 \rightarrow 2} = 5.81 \times 10^{-2}$, which is between D_1 and D_2 , but this value is incorrect because it is significantly different from the composite experiment $D_{1 \rightarrow 2}$. Least squares optimization was then used to estimate the best fit parameters for a PAF model and this identified $\alpha_1 = 1.06D_1$ and $\alpha_2 = 0.67D_2$, with $\beta_j = D_j - \alpha_j$. The resulting PAF-based solution had $D_{PAF} = 4.64 \times 10^{-2}$, which is very close to the correct value of $D_{1 \rightarrow 2}$. The key points are: (a) that the result of the composite (Domain 1 flowing into Domain 2) exhibits different behaviors than either domain individually, (b) that the PAF model is able to describe each experiment accurately and also the composite experiment using consistent parameters, and (c) a PDF-based model would require a new effective spreading coefficient to describe the composite domain. The main limitation here is that least squares optimization had to be used in order to estimate the parameters of the PAF model and nonuniqueness may exist, but some level of fitting/optimization is often needed for any kind of data. In this case, the ratio of parameters is known from the value of $D_{1 \rightarrow 2}$ (see Equation 9), which restricts the values of α_j and β_j to a curve.

The cause of the destructive interference is linked to two factors that are illustrated in Figure 6: (a) each part of the composite domain has similar but distinct velocity distributions (Figure 6a) and (b) velocity correlations are disrupted at the composite interface (Figure 6b). The flux-weighted velocity PDF of the composite domain was used to compute the velocity correlations because it provides a reliable analog for the Lagrangian velocities (trajectories) (Aquino & Le Borgne, 2021; Dentz et al., 2016). S-Lagrangian velocity correlation

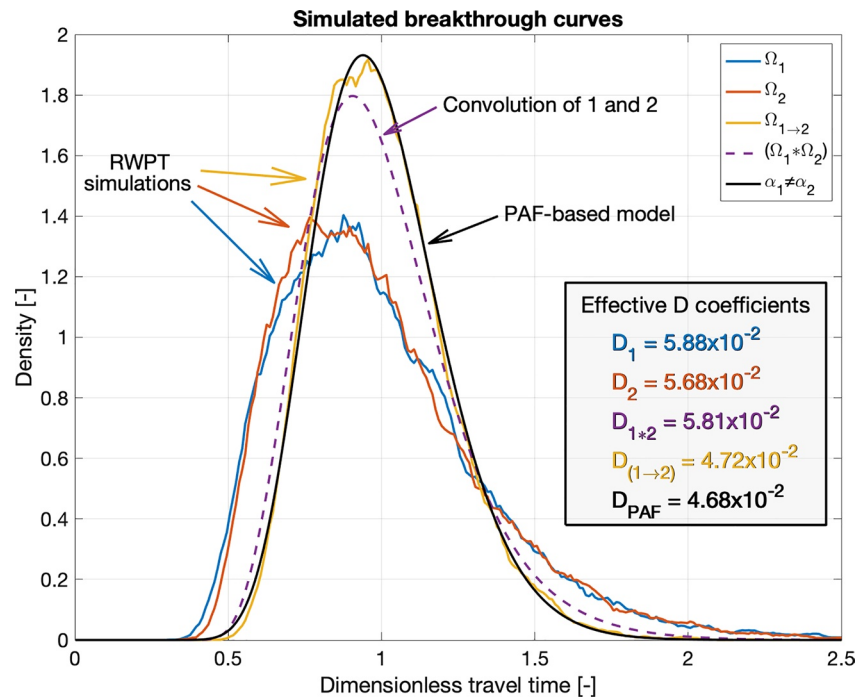


Figure 5. Simulated breakthrough curves for Domain 1 (Ω_1) and Domain 2 (Ω_2), the composite flow experiment ($\Omega_{1 \rightarrow 2}$), the convolution of the breakthrough from Domain 1 and 2 (Ω_{1*2}), and the probability-amplitude function (PAF) based model with nonuniform coefficients. The PAF models applied to either Domain 1 or Domain 2 recover those breakthrough curves with high accuracy, but the PAF is also able to adjust its behavior automatically to describe the interaction of the two domains. Note that composite domain was twice as long and that all were normalized by mean travel time to facilitate comparisons.

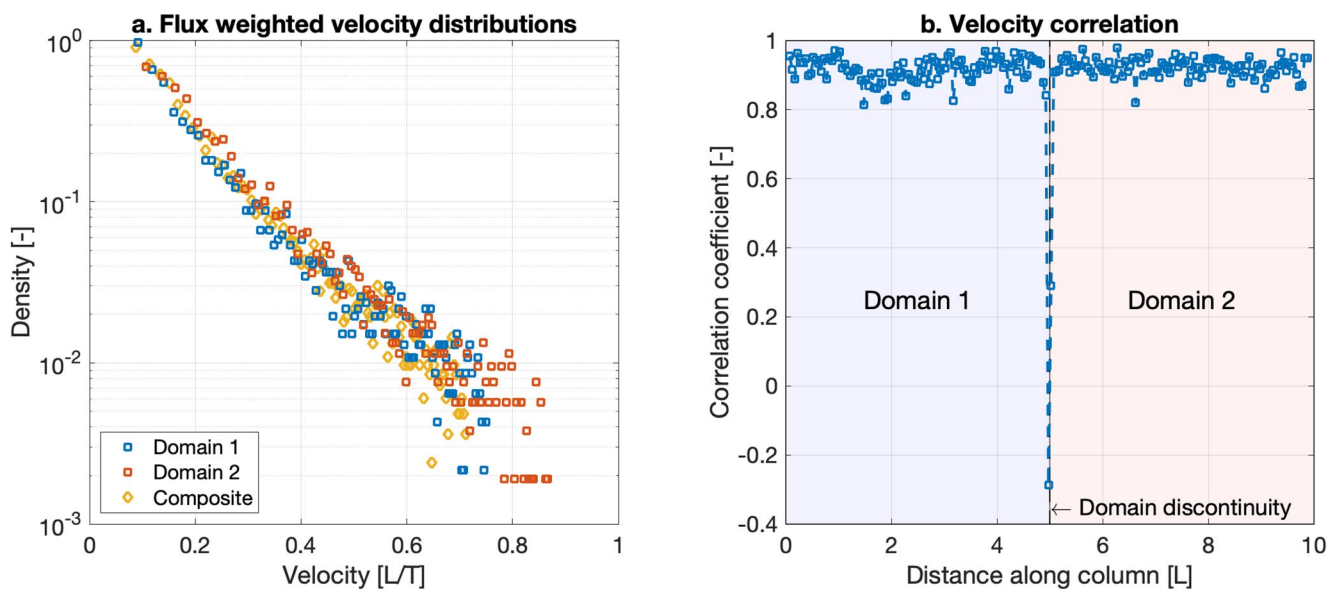


Figure 6. (a) Flux weighted velocity distributions for Domain 1, Domain 2, and the composite domain, and (b) 1d velocity correlation along the column. The velocity distributions are distinct but similar overall. Importantly, there are strong Lagrangian velocity correlations throughout the composite domain. However, the sharp discontinuity between the sub-domains disrupts the otherwise stable correlation leading to destructive interference and reduced spreading.

(Le Borgne et al., 2008) was computed throughout the composite domain, evaluated at a distance of one model cell-size (i.e., Δx). The laterally averaged correlation coefficient as a function of 1d distance along the column is plotted in Figure 6b. The correlation plot shows clearly that there is a high degree of velocity correlation (greater than 0.8) everywhere in the composite domain except at the interface between the two sub-domains. These results provide one possible reason why the PAFs in Domain 1 and Domain 2 are slightly different (small differences in velocity PDFs), and also why their juxtaposition causes a change in the system's behavior, but alternative explanations could also exist.

6. Discussion

The primary purpose of this work has been to evaluate whether or not an amplitude-based model could be applied to model ADE processes with linear transfer functions (operators). The results show that PAF-based propagation can be used for at least one water resource application and that some interesting behaviors become possible when one does so. The significance of those behaviors can be seen by recalling the standard, continuum mechanical approach, which is based on volume averaging and/or upscaling (e.g., Wood, 2009). The continuum mechanical approach averages out all variability that is below the “support scale” of the continuum, meaning that two blocks of porous media with the same parameter values, for example D , are identical in every way despite any sub-continuum differences. Borrowing from the mathematical tools used to describe quantum systems, the PAF approach allows us to define propagators, which recognize that some blocks may indeed have the same macroscopic parameter values, but perhaps for different reasons, and the PAF is able to keep them distinct. In other words, seemingly equivalent blocks of equivalent porous media (in a continuum mechanical sense) are not forced to become identical artificially.

Even without the example of Section 5, there is already evidence that supports the notion of sub-continuum heterogeneity that is remarkably common, some of which is also “unobservable.” For example, the routine decomposition of a 1d hydrodynamic dispersion coefficient into a longitudinal dispersivity and a molecular diffusion term as $D = \alpha_L v + D^*$, respectively (Charbeneau, 2006). This “sub-division” of the spreading processes cannot be observed in a simple laboratory column experiment because only the net impact of both is visible. The molecular diffusion term itself is also potentially nonunique because it represents an *effective* diffusion rate that is impacted by the tortuosity and porosity of the media, and this too may not be directly observable at continuum scales. Furthermore, even using an idealized conceptual model like a bundle of capillary tubes (de Marsily, 1986), two adjacent, identical bundles with one feeding into the next would also interfere with each other if some of the capillaries are not perfectly aligned. Therefore, despite the unique mathematical description employed herein, the concepts of destructive interference and sub-continuum heterogeneity are not themselves new. What is novel is the way that we have used PAFs to embed this sub-continuum heterogeneity into an analytical model of transport, and our demonstration of this property using a realistic numerical example.

There remain some open conceptual questions like, what is the physical interpretation of the complex portion of the PAF and can models like this be derived from first principles? The latter could probably be accomplished with random walks that incorporate those correlations (e.g., Dentz et al., 2016; Le Borgne et al., 2008) and the former might be linked to “momentum-like” effects caused by velocity correlation. The extensive evidence for the importance of velocity correlation across a broad range of transport applications (e.g., Engdahl & Bolster, 2020; Kang et al., 2014, 2015; Morales et al., 2017; Sherman et al., 2019) implies that it is an important factor that should be included when conditioning/calibrating flow models, but, for now, such topics are left for future study. There are also some practical issues like how to obtain model parameters in the field, but creative experimentation may be able to overcome this (e.g., Equation 9) and further development of theories like this could aid in those designs. Even the model shown above is but one possibility to account for “interference effects.” Alternative descriptions using different complex operators may exist and could even be better suited to the task. Given the unique behaviors demonstrated with a PAF here, it seems reasonable to continue exploring more ways to leverage some of the broad conceptual and mathematical tools used in quantum mechanics into hydrogeologic problems; this is in contrast to more literal applications of quantum theory or quantum field theory (e.g., Sposito, 2001). New operators and/or propagators may need to be defined, and a state function approach might give rise to new kinds of upscaling methods, but the main point is that these results suggest that borrowing “quantum-like” tools could lead to

new descriptive and predictive representations of subsurface flow and transport systems. If those tools can be leveraged to develop “quantum upscaled” models for more general water resource problems, such simulations could be posed directly in the natural language of quantum computing. Perhaps this perspective is idealistic, but it is not trivial because it could mean that quantum computers might actually become viable tools for expanding the frontiers and possibilities of hydrologic simulations in the near future.

Appendix A: Analytical Demonstration of Amplitude Interference

The effects seen in Section 4 result from the interference of the state functions when the relative amount of spreading assigned to each of the amplitude components do not match. This behavior is analogous to the constructive/destructive interference that creates wave packets common in quantum mechanics (Bohm, 1951). Here, we show the basic property analytically for functions similar to Equation 5, since handling Equation 5 directly through Laplace transforms involves modified Bessel functions of the second kind and is extraordinarily cumbersome. A much simpler function with all of the necessary properties is the following Galilei invariant state function

$$\gamma_j(x, t) = \frac{1}{\sqrt{t\zeta_j}} \exp\left[-\frac{x^2}{2t\zeta_j}\right] \quad (\text{A1})$$

where $\zeta_j = \alpha_j + i\sqrt{\alpha_j\beta_j}$. A temporal propagator may be defined by taking the Fourier transform (FT) with respect to position, x , resulting in

$$\hat{\gamma}_j(k | \Delta t) = \exp\left[\frac{-\Delta tk^2\zeta_j}{2}\right] \quad (\text{A2})$$

where $x \rightarrow k$ by the FT ($k \in \mathbb{C}$), and we denote this as conditional to an increment of time, $t \rightarrow \Delta t$ since it alters a spatial distribution at fixed intervals of time. Note that we chose the FT here, since the convolution theorem applies to both the FT and the LT, and the FT of this distribution is more manageable analytically; this is also the reason why this example uses a temporal propagator instead of spatial one (e.g., Equation 8). Two successive applications of $\hat{\gamma}_j(k | \Delta t)$ with identical α and β coefficients give

$$\hat{\gamma}_j\hat{\gamma}_j = \exp\left[-\Delta tk^2\zeta_j\right] \quad (\text{A3})$$

and inverting the FT transform yields

$$\gamma(x | 2\Delta t) = \frac{1}{\sqrt{2\Delta t\zeta_j}} \exp\left[-\frac{x^2}{4\Delta t\zeta_j}\right] \quad (\text{A4})$$

which is the same as the evaluating Equation A1 at $2\Delta t$ as we know it should be.

However, if two different ζ , denoted ζ_1 and ζ_2 , are used instead, we obtain the following in Fourier space

$$\hat{\gamma}_1\hat{\gamma}_2 = \exp\left[-\frac{\Delta tk^2}{2}(\zeta_1 + \zeta_2)\right] \quad (\text{A5})$$

which inverts to

$$\gamma_{1,2}(x | 2\Delta t) = \frac{1}{\sqrt{\Delta t(\zeta_1 + \zeta_2)}} \exp\left[-\frac{x^2}{2\Delta t(\zeta_1 + \zeta_2)}\right] \quad (\text{A6})$$

Expanding the summation $(\zeta_1 + \zeta_2) = \alpha_1 + i\sqrt{\alpha_1\beta_1} + \alpha_2 + i\sqrt{\alpha_2\beta_2}$, we can see that anytime $\alpha_1 \neq \alpha_2$ and $\beta_2 \neq \beta_1$, subject to $\alpha_j + \beta_j = D$ that Equation A6 will not give the same result as Equation A4, nor will their corresponding PDFs (i.e., ρ_j) match.

Similar properties for nonuniform D can also be shown analytically from the same summation with minor changes. Define $\alpha_j = \eta_j D_j$ and $\beta_j = (1 - \eta_j) D_j$ for $j = 1, 2$ subject to $D_1 \neq D_2$ and $\alpha_j > 0$, then direct substitution and some algebra gives

$$(\zeta_1 + \zeta_2) = D_1 \left[\eta_1 + i\sqrt{\eta_1(1-\eta_1)} \right] + D_2 \left[\eta_2 + i\sqrt{\eta_2(1-\eta_2)} \right] \quad (\text{A7})$$

From this, we see that when $\eta_1 = \eta_2$ one obtains an “even weighting” of the two different macroscopic D values, consistent with classical transfer function models, but destructive interference occurs when $\eta_1 \neq \eta_2$.

Appendix B: Multiple Spatial Dimensions

The PAF used in this article is based on a 1d upscaled model, but it is possible to extend the approach to multiple dimensions. Since this can be done in many ways, just two examples are included for brevity but these illustrate the main considerations for n -dimensional applications.

The first example is for purely diffusive spreading and is based on the general solution for diffusion in n -dimensional space. The Green’s function for the real-space (classical) solution centered at the origin is given by

$$g(\mathbf{x}, t) = \frac{\exp\left[-\frac{1}{4t} \mathbf{x}^T \mathbf{D}^{-1} \mathbf{x}\right]}{\sqrt{(4\pi t)^d \det(\mathbf{D})}} \quad (\text{B1})$$

where \mathbf{x} is an n -d position vector, \mathbf{D} is an $n \times n$ spreading tensor, T is the transpose operator, \det is the determinant operator, and $d = 1, 2, 3$ is the dimensionality (Bolster et al., 2011). Allowing for a diagonal spreading tensor with the n -d diagonal components denoted as D_j , a PAF can be defined as

$$\psi(\mathbf{x}, t) = \frac{\exp\left[-\frac{1}{8t} \mathbf{x}^T \mathbf{K}^{-1} \mathbf{x}\right]}{\left[(4\pi t)^d \det(\mathbf{A})\right]^{1/4}} \quad (\text{B2})$$

requiring that the nonzero (i.e., diagonal) values of the tensors \mathbf{A} and \mathbf{K} are given by $A(j, j) = \alpha_j + \beta_j$ and $K(j, j) = \alpha_j + i\sqrt{\alpha_j \beta_j}$. Complex conjugation of Equation B2 recovers Equation B1.

The second example is the flow along a 1d streamline with longitudinal and transverse spreading, creating a 3d spreading model. The real-space PDF can be built from the product of three 1d Green’s functions, which is assumed to have independent rates (i.e., a diagonal spreading tensor). Following Charbeneau (2006) for a 3d coordinate system with directions denoted as x, y, z , the kernels are

$$g_x(x, t) = \frac{\exp\left[\frac{-(x-vt)^2}{4D_x t}\right]}{\sqrt{4\pi D_x t}}, \quad g_y(y, t) = \frac{\exp\left[\frac{-(y)^2}{4D_y t}\right]}{\sqrt{4\pi D_y t}}, \quad g_z(z, t) = \frac{\exp\left[\frac{-(z)^2}{4D_z t}\right]}{\sqrt{4\pi D_z t}} \quad (\text{B3})$$

The corresponding PAFs are

$$\psi_x(x, t) = \frac{\exp\left[\frac{-(x-vt)^2}{8t(\alpha_x + i\sqrt{\alpha_x \beta_x})}\right]}{\left[4\pi(\alpha_x + \beta_x)t\right]^{1/4}}, \quad \psi_y(y, t) = \frac{\exp\left[\frac{-(y)^2}{8t(\alpha_y + i\sqrt{\alpha_y \beta_y})}\right]}{\left[4\pi(\alpha_y + \beta_y)t\right]^{1/4}}, \quad (\text{B4})$$

The z direction term is omitted for brevity but it should be clear that its form is analogous to the y direction model. Summation of the kernels, or PAFs, produces the multi-dimensional model (Charbeneau, 2006).

Regardless of which case one adopts, the PAFs (Equations B2 or B4) may then be subjected to linear operators (convolution) to create a wide range of solutions, which can then be transformed into PDFs through complex conjugation. The main challenge of any n -d model is the added difficulty in identifying the parameters; hence the use of 1d methods in this article. However, the point is that it is possible to generalize the PAF to multiple spatial dimensions.

Conflict of Interest

The author has no potential conflicts of interest to declare.

Acknowledgments

Support for this work was provided by the US Department of Energy, Office of Science under award DE-SC0019123 and the National Science Foundation under award EAR-2049687. Results may be generated analytically using the equations herein.

References

Aquino, T., & Le Borgne, T. (2021). The diffusing-velocity random walk: A spatial-Markov formulation of heterogeneous advection and diffusion. *Journal of Fluid Mechanics*, 910(A12). <https://doi.org/10.1017/jfm.2020.957>

Atchley, A. L., Maxwell, R. M., & Navarre-Sitchler, A. K. (2013). Using streamlines to simulate stochastic reactive transport in heterogeneous aquifers: Kinetic metal release and transport in CO₂ impacted drinking water aquifers. *Advances in Water Resources*, 52, 93–106. <https://doi.org/10.1016/j.advwatres.2012.09.005>

Bohm, D. (1951). *Quantum theory*. Dover Books on Physics.

Bolster, D., Dentz, M., & Le Borgne, T. (2011). Hypermixing in linear shear flow. *Water Resources Research*, 47(9), 1–5. <https://doi.org/10.1029/2011WR010737>

Carslaw, H. S., & Jaeger, J. C. (1959). *Conduction of heat in solids* (2nd ed.). Oxford: Oxford University Press.

Charbeneau, R. (2006). *Groundwater hydraulics and pollutant transport* (1st ed.). Waveland Press, Inc.

Cvetkovic, V., Carstens, C., Selroos, J.-O., & Destouni, G. (2012). Water and solute transport along hydrological pathways. *Water Resources Research*, 48(6), W06537. <https://doi.org/10.1029/2011WR011367>

Dagan, G. (1990). Transport in heterogeneous porous formations: Spatial moments, ergodicity, and effective dispersion. *Water Resources Research*, 26(6), 1281–1290. <https://doi.org/10.1029/WR026i006p01281>

de Marsily, G. (1986). *Quantitative hydrogeology: Groundwater hydrology for engineers* (1st ed.). Academic Press.

Dentz, M., Kang, P. K., Comolli, A., Le Borgne, T., & Lester, D. R. (2016). Continuous time random walks for the evolution of Lagrangian velocities. *Physical Review Fluids*, 1(7), 1–13. <https://doi.org/10.1103/PhysRevFluids.1.074004>

Devanatham, V. (2011). *Relativistic quantum mechanics and quantum field theory* (1st ed.). Oxford, UK: Alpha Science International.

Engdahl, N. B., & Bolster, D. (2020). Markovian transport processes in a heterogeneous, variably saturated watershed: A multi-domain spatial Markov model. *Advances in Water Resources*, 138, 103555. <https://doi.org/10.1016/j.advwatres.2020.103555>

Engdahl, N. B., & Weissmann, G. S. (2010). Anisotropic transport rates in heterogeneous porous media. *Water Resources Research*, 46(2), 1–12. <https://doi.org/10.1029/2009WR007910>

Gelhar, L. W., & Axness, C. L. (1983). Three-dimensional stochastic analysis of macrodispersion in aquifers. *Water Resources Research*, 19(1), 161–180. <https://doi.org/10.1029/WR019i001p00161>

Ginn, T. R. (2001). Stochastic-convective transport with nonlinear reactions and mixing: Finite streamtube ensemble formulation for multicomponent reaction systems with intra-streamtube dispersion. *Journal of Contaminant Hydrology*, 47(1), 1–28. [https://doi.org/10.1016/S0169-7722\(00\)00167-4](https://doi.org/10.1016/S0169-7722(00)00167-4)

Ginn, T. R., Schreyer, L. G., & Zamani, K. (2017). Phase exposure-dependent exchange. *Water Resources Research*, 53, 619–632. <https://doi.org/10.1002/2016WR019755>

Green, C. T., Böhlke, J. K., Bekins, B. A., & Phillips, S. P. (2010). Mixing effects on apparent reaction rates and isotope fractionation during denitrification in a heterogeneous aquifer. *Water Resources Research*, 46(8), 1–19. <https://doi.org/10.1029/2009WR008903>

Haggerty, R., & Gorelick, S. M. (1995). Multiple-rate mass transfer for modeling diffusion and surface reactions in media with pore-scale heterogeneity. *Water Resources Research*, 31(10), 2383–2400. <https://doi.org/10.1029/95wr10583>

Hammond, G. E., & Lichtner, P. C. (2010). Field-scale model for the natural attenuation of uranium at the Hanford 300 Area using high-performance computing. *Water Resources Research*, 46(9), 1–31. <https://doi.org/10.1029/2009WR008819>

Johnston, E. R., Harrigan, N., & Gimeno-Segovia, M. (2019). *Programming quantum computers: Essential algorithms and code samples* (1st ed.). Sebastopol, CA: O'Reilly Media, Inc.

Kang, P. K., De Anna, P., Nunes, J. P., Bijeljic, B., Blunt, M. J., & Juanes, R. (2014). Pore-scale intermittent velocity structure underpinning anomalous transport through 3-D porous media. *Geophysical Research Letters*, 41, 6184–6190. <https://doi.org/10.1002/2014GL061475>

Kang, P. K., Le Borgne, T., Dentz, M., Bour, O., & Juanes, R. (2015). Impact of velocity correlation and distribution on transport in fractured media: Field evidence and theoretical model. *Water Resources Research*, 51, 940–959. <https://doi.org/10.1002/2014WR015799>

Kollet, S. J., Maxwell, R. M., Woodward, C. S., Smith, S., Vanderborght, J., Vereecken, H., & Simmer, C. (2010). Proof of concept of regional scale hydrologic simulations at hydrologic resolution utilizing massively parallel computer resources. *Water Resources Research*, 46(4), 1–7. <https://doi.org/10.1029/2009WR008730>

Le Borgne, T., Dentz, M., & Carrera, J. (2008). Lagrangian statistical model for transport in highly heterogeneous velocity fields. *Physical Review Letters*, 101(9), 1–4. <https://doi.org/10.1103/PhysRevLett.101.090601>

Loschko, M., Wöhling, T., Rudolph, D. L., & Cirpka, O. A. (2016). Cumulative relative reactivity: A concept for modeling aquifer-scale reactive transport. *Water Resources Research*, 52(10), 8117–8137. <https://doi.org/10.1002/2016WR019080>

Massoudieh, A., & Dentz, M. (2020). Upscaling non-linear reactive transport in correlated velocity fields. *Advances in Water Resources*, 143, 103680. <https://doi.org/10.1016/j.advwatres.2020.103680>

Maxwell, R. M., Condon, L. E., & Kollet, S. J. (2015). A high-resolution simulation of groundwater and surface water over most of the continental US with the integrated hydrologic model ParFlow v3. *Geoscientific Model Development*, 8(3), 923–937. <https://doi.org/10.5194/gmd-8-923-2015>

Maxwell, R. M., Tompson, A. F. B., & Kollet, S. (2009). A serendipitous, long-term infiltration experiment: Water and tritium circulation beneath the CAMBRIC trench at the Nevada Test Site. *Journal of Contaminant Hydrology*, 108(1–2), 12–28. <https://doi.org/10.1016/j.jconhyd.2009.05.002>

Maxwell, R. M., Welty, C., & Tompson, A. F. B. (2003). Streamline-based simulation of virus transport resulting from long term artificial recharge in a heterogeneous aquifer. *Advances in Water Resources*, 26(10), 1075–1096. [https://doi.org/10.1016/S0309-1708\(03\)00074-5](https://doi.org/10.1016/S0309-1708(03)00074-5)

McQuarrie, D. A., & Simon, J. D. (1997). *Physical chemistry: A molecular approach*. Sausalito, CA: University Science Books.

Morales, V. L., Dentz, M., Willmann, M., & Holzner, M. (2017). Stochastic dynamics of intermittent pore-scale particle motion in three-dimensional porous media: Experiments and theory. *Geophysical Research Letters*, 44, 9361–9371. <https://doi.org/10.1002/2017GL074326>

Neuman, S. P., & Tartakovsky, D. M. (2009). Perspective on theories of non-Fickian transport in heterogeneous media. *Advances in Water Resources*, 32(5), 670–680. <https://doi.org/10.1016/j.advwatres.2008.08.005>

Neuman, S. P., Winter, C., & Newman, C. (1987). Stochastic theory of field-scale Fickian dispersion in anisotropic porous media. *Water Resources Research*, 23(3), 453–466. <https://doi.org/10.1029/wr023i003p00453>

- Ogata, A., & Banks, R. (1961). *A solution of the differential equation of longitudinal dispersion in porous media* (pp. A1–A7). Geological Survey (U.S.). Retrieved from <http://pubs.er.usgs.gov/publication/pp411A>
- Riazuddin, F. (2013). *Quantum mechanics* (2nd ed.). Singapore: World Scientific Publishing.
- Riva, M., & Guadagnini, A. (2009). Effects of evolving scales of heterogeneity on hydraulic head predictions under convergent flow conditions. *Hydrogeology Journal*, 17(4), 817–825. <https://doi.org/10.1007/s10040-008-0396-9>
- Sherman, T., Engdahl, N. B., Porta, G., & Bolster, D. (2020). A review of spatial Markov models for predicting pre-asymptotic and anomalous transport in porous and fractured media. *Journal of Contaminant Hydrology*, 236. <https://doi.org/10.1016/j.jconhyd.2020.103734>
- Sherman, T., Roche, K. R., Richter, D. H., Packman, A. I., & Bolster, D. (2019). A dual domain stochastic Lagrangian model for predicting transport in open channels with hyporheic exchange. *Advances in Water Resources*, 125, 57–67. <https://doi.org/10.1016/j.advwatres.2019.01.007>
- Silva, O., Carrera, J., Dentz, M., Kumar, S., Alcolea, A., & Willmann, M. (2009). A general real-time formulation for multi-rate mass transfer problems. *Hydrology and Earth System Sciences*, 13(8), 1399–1411. <https://doi.org/10.5194/hess-13-1399-2009>
- Simmons, C. S. (1982). A stochastic-convective transport representation of dispersion in one-dimensional porous media systems. *Water Resources Research*, 18(4), 1193–1214. <https://doi.org/10.1029/WR018i004p01193>
- Simmons, C. S., Ginn, T. R., Wood, B. D., & Wood, B. D. (1995). Stochastic-convective transport with nonlinear reaction: Mathematical framework. *Water Resources Research*, 31(11), 2675–2688. <https://doi.org/10.1029/95WR02178>
- Sposito, G. (2001). Methods of quantum field theory in the physics of subsurface solute transport. *Transport in Porous Media*, 42, 181–198. https://doi.org/10.1007/978-94-017-1278-1_9
- Weissmann, G. S., Zhang, Y., LaBolle, E. M., & Fogg, G. E. (2002). Dispersion of groundwater age in an alluvial aquifer system. *Water Resources Research*, 38(10). <https://doi.org/10.1029/2001WR000907>
- Wood, B. D. (2009). The role of scaling laws in upscaling. *Advances in Water Resources*, 32(5), 723–736. <https://doi.org/10.1016/j.advwatres.2008.08.015>
- Zhang, Y., Benson, D. A., Meerschaert, M. M., & LaBolle, E. M. (2007). Space-fractional advection-dispersion equations with variable parameters: Diverse formulas, numerical solutions, and application to the Macrodispersion Experiment site data. *Water Resources Research*, 43(5), 1–16. <https://doi.org/10.1029/2006WR004912>